Physics Letters B 816 (2021) 136275

Contents lists available at ScienceDirect

Physics Letters B

www.elsevier.com/locate/physletb

First microscopic evaluation of spin-dependent WIMP-nucleus scattering off ^{183}W

P. Pirinen [a,*], J. Kotila [b,c], J. Suhonen [a]

[a] University of Jyväskylä, Department of Physics, P. O. Box 35 (YFL), FI-40014, Finland
[b] Finnish Institute for Educational Research, University of Jyväskylä, P.O. Box 35, FI-40014 Jyväskylä, Finland
[c] Center for Theoretical Physics, Sloane Physics Laboratory, Yale University, New Haven, CT 06520-8120, USA

ARTICLE INFO

Article history:
Received 20 January 2021
Received in revised form 29 March 2021
Accepted 30 March 2021
Available online 2 April 2021
Editor: W. Haxton

Keywords:
Dark matter
WIMP
Direct detection
Interacting boson-fermion model
Nuclear structure
Spin structure functions

ABSTRACT

We perform the first consistent calculation of elastic-scattering and inelastic-scattering structure functions for spin-dependent WIMP-nucleus scattering off ^{183}W in a microscopic nuclear-theory framework. The nuclear structure calculations are performed in the microscopic interacting boson-fermion model (IBFM-2). Our results show that while ^{183}W is very insensitive to spin-dependent elastic scattering, the structure function for inelastic scattering is quite sizable at small momentum transfers. Moreover, to our knowledge ^{183}W provides the first studied case where inelastic scattering can compete with elastic scattering as the primary detection signal.

1. Introduction

The hunt for dark matter intensifies, as detectors get progressively larger and more efficient at catching the most elusive of nature's particles. The race to find the missing mass of the universe in the form of Weakly Interacting Massive Particles (WIMPs) is led by tonne-scale liquid-xenon detectors [1,2], attempting to detect interactions of WIMPs with atomic nuclei. Complementary direct-detection efforts can still probe different parts of the dark matter parameter space, and several such approaches exist.

To evaluate the WIMP-nucleus scattering event rate in a detector, one must account for the structure of the nucleus via a structure function. Reliable estimates for structure functions require a realistic model for the nucleus, and such calculations have typically been performed in the nuclear shell model [3–14]. While most nuclei currently used in dark matter detectors have been examined in detail, tungsten, used currently in the $CaWO_4$ crystals of the CRESST detector, still lacks decent theoretical description. The heavy tungsten lies in a region of deformed nuclei, providing a challenge for nuclear models. Approximations of spin-dependent elastic scattering of WIMPs off ^{183}W have been made before using a simple odd-group model [15]. Here we present the first calculation of structure functions for ^{183}W within a complete microscopic nuclear framework. We use the microscopic Interacting Boson-Fermion Model (IBFM-2), which is designed to handle deformed nuclei in a systematic way by using spectroscopic data to pin down the details of the model Hamiltonian for a given region of nuclei of interest. The formalism was benchmarked recently with well-established detector nuclei, and it was shown to have reasonable accuracy when compared with earlier calculations in the nuclear shell model [16].

Great progress has been made in recent years in evaluating spin structure functions based on axial-vector currents derived from chiral effective field theory [9,10,17,18]. Refs. [9,10] included for the first time the effect of the leading long-range two-body currents, which in general act to decrease the spin-dependent WIMP-nucleus cross section at low momentum transfers. In Ref. [17] all one-body and two-body currents relevant to WIMP-nucleus scattering were derived. Consequently, Ref. [18] very recently added all pion-exchange, pion-pole, and contact currents into the formalism of Refs. [9,10]. In this article, we utilize this formalism to perform the first calculation of spin-dependent structure functions for WIMPs scattering off ^{183}W.

In Section 2 we summarize the essentials of the formalism required to compute spin structure functions for WIMP-nucleus scattering. In Section 3 the IBFM-2 calculation is presented. Results of our calculations are given in Section 4, and in Section 5 we report the conclusions of the present work.

* Corresponding author.
E-mail address: pekka.a.pirinen@jyu.fi (P. Pirinen).

https://doi.org/10.1016/j.physletb.2021.136275

2. Structure functions

We utilize the formalism derived in detail in Refs. [9,10] and used previously in conjunction with the IBFM in Ref. [16]. For convenience, we summarize the main parts again here with updates to the two-body currents from Refs. [17,18]. The spin-dependent WIMP-nucleus cross section can be written as [19]

$$\frac{d\sigma}{dq^2} = \frac{8G_F^2}{(2J_i+1)v^2} S_A(q), \tag{1}$$

where G_F is the Fermi coupling constant, v is the speed of the WIMP in the laboratory frame, and q is the momentum transfer from the nucleus to the WIMP. S_A is the axial-vector structure function, expanded in a multipole decomposition as

$$S_A(q) = \sum_{L\geq 0} \left|\langle J_f||\mathcal{L}_L^5(q)||J_i\rangle\right|^2 + \sum_{L\geq 1}\left(\left|\langle J_f||\mathcal{T}_L^{\mathrm{el5}}(q)||J_i\rangle\right|^2 + \left|\langle J_f||\mathcal{T}_L^{\mathrm{mag5}}(q)||J_i\rangle\right|^2\right). \tag{2}$$

Here the usual longitudinal, transverse electric, and transverse magnetic multipole operators are [10]

$$\mathcal{L}_L^5(q) = \frac{i}{\sqrt{2L+1}}\sum_{i=1}^{A}\frac{1}{2}\left[a_0 + a_1\tau_i^3\left(1+\delta a_1(q) - \frac{2g_{\pi pn}F_\pi q^2}{2m_p g_A(q^2+m_\pi^2)} + \delta a_1^P(q)\right)\right] \times\left[\sqrt{L+1}M_{L,L+1}(q\mathbf{r}_i) + \sqrt{L}M_{L,L-1}(q\mathbf{r}_i)\right], \tag{3}$$

$$\mathcal{T}_L^{\mathrm{el5}}(q) = \frac{i}{\sqrt{2L+1}}\sum_{i=1}^{A}\frac{1}{2}\left[a_0 + a_1\tau_i^3\left(1 - \frac{2q^2}{\Lambda_A^2} + \delta a_1(q)\right)\right] \times\left[-\sqrt{L}M_{L,L+1}(q\mathbf{r}_i) + \sqrt{L+1}M_{L,L-1}(q\mathbf{r}_i)\right], \tag{4}$$

and

$$\mathcal{T}_L^{\mathrm{mag5}}(q) = \frac{i}{\sqrt{2L+1}}\sum_{i=1}^{A}\frac{1}{2}\left[a_0 + a_1\tau_i^3\left(1 - \frac{2q^2}{\Lambda_A^2} + \delta a_1(q)\right)\right] M_{L,L}(q\mathbf{r}_i), \tag{5}$$

where $F_\pi = 92.4$ MeV is the pion decay constant, $m_\pi = 138.04$ MeV the pion mass, $m_p = 938.27$ MeV the proton mass, $\Lambda_A = 1040$ MeV the axial mass parameter, $g_A = 1.27641(56)$ [20] the axial-vector coupling constant, and $g_{\pi pn} = 13.05$ the strong pion-nucleon coupling constant [10]. The operator $M_{L,L'}$ is defined as $M_{L,L'} = j_{L'}(qr_i)[Y_{L'}(\hat{\mathbf{r}}_i)\sigma_i]_L$, where $j_{L'}$ is a spherical Bessel function, $Y_{L'}$ a spherical harmonic, and σ a Pauli spin operator.

The coefficients $\delta a_1(q)$ and $\delta a_1^P(q)$ contain the isovector contribution of two-body currents from chiral EFT at the normal-ordered one-body level. We use the updated two-body currents of Ref. [17] which include all pion-exchange, pion-pole, and contact terms leading to [18]

$$\delta a_1(q) = -\frac{\rho}{F_\pi^2}\left[\frac{1}{3}\left(c_4 + \frac{1}{4m_p}\right)\left[3I_2^\sigma(\rho,q) - I_1^\sigma(\rho,q)\right] - \frac{1}{3}\left(c_3 - \frac{1}{4m_p}\right)I_1^\sigma(\rho,q) - \left(\frac{1+\hat{c}_6}{12m_p}\right)I_{c6}(\rho,q) - \frac{c_D}{4g_A\Lambda_\chi}\right] \tag{6}$$

and

$$\delta a_1^P(q) = \frac{\rho}{F_\pi^2}\left[-2(c_3-2c_1)\frac{M_\pi^2 q^2}{(m_\pi^2+q^2)^2} + \frac{c_3+c_4}{3}I^P(\rho,q) - \left(\frac{1+\hat{c}_6}{12m_p} - \frac{2}{3}\frac{c_1 M_\pi^2}{M_\pi^2+q^2}\right)I_{c6}(\rho,q) - \frac{q^2}{M_\pi^2+q^2}\left[\frac{c_3}{3}[I_1^\sigma(\rho,q) + I^P(\rho,q)] + \frac{1}{3}\left(c_4 + \frac{1}{4m_p}\right)\times[I_1^\sigma(\rho,q) + I^P(\rho,q) - 3I_2^\sigma(\rho,q)]\right] - \frac{c_D}{4g_A\Lambda_\chi}\frac{q^2}{M_\pi^2+q^2}\right]. \tag{7}$$

Here we use $\Lambda_\chi = 700$ MeV for the chiral scale. For the density we adopt a range of values $\rho = 0.10...0.12$ fm^{-1}. Expressions for the integrals I_1^σ, I_2^σ, I_{c6}, and I^P are derived in Ref. [10] and for a revision of the general formalism, we refer the reader to Ref. [18].

The coefficients c_i and c_D are low-energy constants (LECs) that arise from the chiral expansion. It is noteworthy that we use the convention of Ref. [10] where relativistic correction factors proportional to $\frac{1}{m_p}$ in c_4 and $\hat{c}_6$ are explicitly written out in Eqs. (6)–(7) and $\hat{c}_6$ is written in a dimensionless form following Refs. [10,21]. This is different from the convention of Ref. [18] where the relativistic correction factors were absorbed into the LECs. Taking the difference in conventions into account, we use the values of Ref. [18] for c_1, c_3, and c_4 based on the Roy-Steiner equation analysis of Ref. [22]. The value of $\hat{c}_6 = 5.83$ was taken from Ref. [21]. We note that the results shown in this paper are essentially independent of changes in $\hat{c}_6$ within any reasonable range of values and any uncertainty in $\hat{c}_6$ is thus ignored.

The value of c_D is not as readily pinned down. An argument can be made from the notion that two-body currents should account for the quenching of Gamow-Teller beta decay matrix elements in the shell model led by axial-vector currents at zero momentum transfer [18]. However, we are not confident in expanding the idea to a heavy deformed nucleus in the IBFM-2, and opt to use a conservative range of values $-8.0 \leq c_D \leq 2.0$ instead. This range contains most of the values obtained for c_D in relevant literature [18,23–26]. In addition we also present all results with the contact terms turned off with $c_D = 0$. For recoil energies $E_R \geq 40$ keV the uncertainty in c_D becomes the leading accountable uncertainty in our calculations for elastic scattering. The values of the low-energy constants used in our calculations are summarized in Table 1.

Table 1
Values of the low-energy constants (LECs) used in this work. Values of c_1, c_3, and c_4 were taken from Ref. [18], $\hat{c}_6$ from [21], and the range of c_D was chosen to represent reasonable values used in other works (see text).

LEC	Value
c_1	$-1.20(17)$ GeV^{-1}
c_3	$-4.45(86)$ GeV^{-1}
c_4	$2.69(70)$ GeV^{-1}
$\hat{c}_6$	5.83
c_D	$-8.0...2.0$

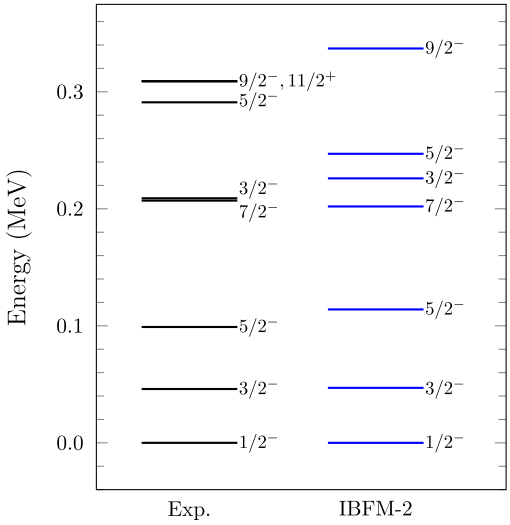

Fig. 1. Experimental and IBFM-2-computed energy spectra for ^{183}W. Only negative-parity states were computed in the IBFM-2.

3. IBFM-2 calculation

For the IBFM-2 calculation the even-even ^{184}W nucleus was used as core for the odd ^{183}W nucleus. The IBM-2 parameters for the core tungsten nucleus, described as four proton bosons and eight neutron bosons, were taken from Ref. [27]. The valence space was chosen to span $0g_{7/2}$, $1d_{5/2}$, $1d_{3/2}$, $2s_{1/2}$, and $0h_{11/2}$ proton and $0h_{9/2}$, $1f_{7/2}$, $1f_{5/2}$, $2p_{3/2}$, $2p_{1/2}$, and $0i_{13/2}$ neutron orbitals. The single-particle energies for protons were taken from [28], where the effect of single-particle energies on occupation probabilities was studied. The occupation probabilities and quasiparticle energies for neutrons were taken from [29] where odd tungsten isotopes were studied by means of IBFM-1. Finally, the used boson-fermion interaction parameters for negative-parity states read as $\Gamma_\rho = -0.1285$, $\Lambda_\rho = 0.004$ and $A_\rho = -0.131$. The obtained low-energy spectrum for negative-parity states is shown in Fig. 1, and it corresponds very well to the experimental spectrum.

The mapping of the single-fermion creation operator onto the IBFM-2 space follows the procedure introduced in Ref. [30] where evaluation of the relevant terms using exact values for the fermion matrix elements in the Generalized Seniority scheme was worked out without using the Number Operator Approximation (NOA). For the even numbered nucleons, protons for ^{183}W, the mapping procedure of the shell model into the microscopic IBM is described in detail in Refs. [31,32], and more recently in Ref. [33] in connection with double-beta-decay studies and in Ref. [28] for calculating occupation probabilities. Basically, the shell-model creation operators of collective pairs of nucleons of pair angular momenta 0 and 2, the S and D pairs, are used to span the SD fermion space, which is a subspace of the full shell-model space. The states of the SD subspace are then mapped onto boson states belonging to the IBM space.

Although it is generally accepted that the SD-pair approximation is valid in the spherical and vibrational regions where seniority is approximately conserved, the situation is more complicated when describing rotational states in the deformed region, as in the current case of ^{183}W. Thus, the used Otsuka-Arima-Iachello (OAI) mapping [32] may not be optimal and we recognize the uncertainty this adds to our results. In particular, higher order interactions may be necessary since in principle any fermion operator in the fermion subspace can be mapped exactly onto the corresponding operator in the boson space at the expense of introducing higher order boson interactions. Alternatively, another type of boson mapping could be employed and tested.

4. Results

In this section we will present the computed spin structure functions for WIMP-nucleus scattering off ^{183}W. We will consider both elastic scattering and inelastic scattering populating the first $3/2^-$ state. First, however, we will start by evaluating magnetic observables involving the spin operator to roughly assess the uncertainty in our nuclear model.

The ground-state magnetic moment of ^{183}W in our IBFM-2 calculation is $+0.315\ \mu_N$ while the experimental value is $+0.11778476(9)\ \mu_N$ [34]. The computed M1 transition strength of the gamma transition from the first $3/2^-$ state to the $1/2^-$ ground state is 0.047 W.u., and the measured one is 0.125(5) W.u. [34]. Our calculation appears to overestimate the neutron spin expectation value of the ground state which leads to the large ground-state magnetic moment, and is likely to cause the elastic-scattering spin structure function to be overestimated by a similar factor of 2–3 at zero momentum transfer. Similarly, our calculation slightly underestimates the $B(\mathrm{M1}: 3/2_1^- \rightarrow 1/2_{gs}^-)$ value which suggests that the predicted inelastic-scattering structure functions might also be somewhat smaller than in reality.

We decompose the spin structure function S_A of Eq. (2) to isoscalar and isovector parts:

$$S_A(q) = a_0^2 S_{00}(q) + a_0 a_1 S_{01}(q) + a_1^2 S_{11}(q). \tag{8}$$

We present our results in the conventional form of so-called proton-only ($a_0 = a_1 = 1$) and neutron-only ($a_0 = -a_1 = 1$) couplings:

$$S_p(q) = S_{00}(q) + S_{01}(q) + S_{11}(q), \tag{9}$$

$$S_n(q) = S_{00}(q) - S_{01}(q) + S_{11}(q). \tag{10}$$

The calculated spin structure functions for elastic and inelastic scattering of WIMPs off ^{183}W are shown in Fig. 2 as functions of the nuclear recoil energy $E_R = q^2/(2m_A)$, where m_A is the mass of the nucleus. For convenience, we also give a function fit to S_p and S_n in the Appendix. Here we immediately notice the usual enhancement of the structure function of the even species of nucleons (here protons) by the two-body currents at small momentum transfers. With two-body currents included in the elastic channel, both S_n and S_p at $E_R > 40$ keV quite closely follow the structure function computed with one-body currents only, especially when the contact terms in Eqs. (6)–(7) are ignored by setting $c_D = 0$. In the inelastic channel the two-body currents systematically decrease the value of the "neutron-only" S_n at all E_R. We note that the inelastic channel is very stable to variation in c_D.

Spin-dependent elastic scattering has been deemed an ineffective detection strategy for a detector using ^{183}W due to the small spin expectation value of the ground state estimated in the odd group model [15]. Our analysis verifies this expectation, even when taking into account the fact that our calculation likely overestimates the expectation value by roughly a factor of 2. The structure function of ^{183}W for elastic scattering is at $E_R = 0$ keV an order of magnitude smaller than that of ^{129,131}Xe or ^{125}Te computed in the IBFM-2 [16].

The structure function for inelastic scattering shows promise, however. In contrast to the inelastic scattering structure functions of ^{129,131}Xe computed in the IBFM-2 [16] and the shell model [11], and ^{125}Te computed in the IBFM-2 [16], here the structure function does not fall as E_R approaches zero, but it gets larger. This leads to the structure function being much larger at $E_R = 0$ keV than for any of the nuclei previously studied. Interestingly this is also the

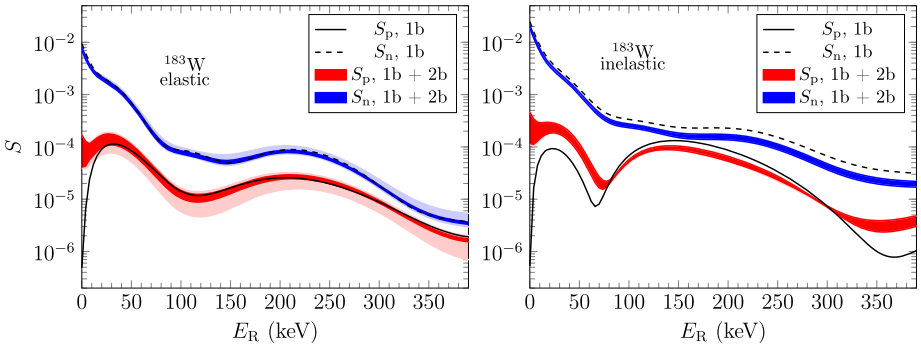

Fig. 2. Elastic (left panel) and inelastic (right panel) spin structure functions for ^{183}W as functions of the recoil energy E_R. Solid and dashed lines represent the one-body-current contributions to the structure function, while the corresponding colored bands show the total structure function with two-body currents included. The thickness of the band is related to the uncertainty in the low-energy constants and the range of densities (see text). The solid colored bands were computed with $c_D = 0$, and the transparent bands were computed with a range of values $-8.0 \leq c_D \leq 2.0$.

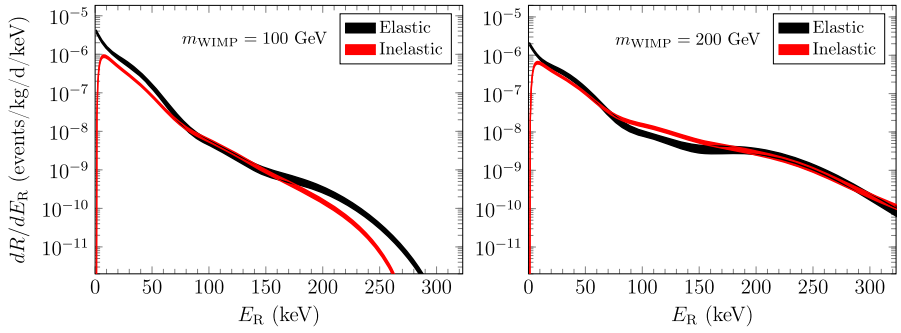

Fig. 3. Differential event rate of elastic and inelastic WIMP-nucleus scattering off ^{183}W for WIMP masses of 100 GeV (left panel) and 200 GeV (right panel). We have assumed "neutron-only" couplings, a WIMP velocity distribution following the standard halo model, and a WIMP-nucleon cross section of 10^{-40} cm^2. The thickness of the curves represents the uncertainty in the low-energy constants involved in the calculation, and we use the large range of values for c_D (see text).

first case where the inelastic structure function at $E_R = 0$ keV is larger than that of the elastic channel.

The wave functions of the ground state and first excited state of ^{183}W in our IBFM-2 calculation are dominated by a neutron on either the $2p_{1/2}$ or $2p_{3/2}$ orbital coupled to a 0^+ or 2^+ boson state. This leads to strong single particle transitions between the neutron $2p$ orbitals in our valence space for the $L = 1$ multipole. These strong single-particle transitions cause the structure function to be large at $E_R = 0$ keV. The experimentally observed M1 transition between the first excited state and ground state of ^{183}W is also stronger than that for ^{125}Te or ^{129,131}Xe, which is likely made possible via the same single-particle transitions between the $2p$ orbitals.

In addition to the structure function, there are kinematical constraints which influence the magnitude and shape of the observed signal in a detector. To gain insight to this, we compute the differential event rate as a function of the recoil energy E_R for elastic and inelastic scattering of WIMPs off a ^{183}W target as described in Ref. [11] (originally from Ref. [35]):

$$\frac{dR}{dE_R} = \frac{\sqrt{\pi}v_0}{2}\frac{R_0}{m_{WIMP}m_A}\frac{g(v_{min})}{E_0 r}\frac{\sigma(E_R)}{10^{-36}\,\text{cm}^2} \times \frac{\rho_0}{0.3\,\text{GeV cm}^{-3}}\frac{v_0}{220\,\text{km s}^{-1}}. \quad (11)$$

Here $R_0 = 361$ events/kg/d, E_0 is the most probable kinetic energy of the WIMP, and $\rho_0 = 0.3$ GeV/cm^3 is the local WIMP density. To evaluate the velocity integral

$$g(v_{min}) = \int_{v_{min}}^{\infty} \frac{f(\mathbf{v}+\mathbf{v}_E)}{v} d^3\mathbf{v}, \quad (12)$$

where $\mathbf{v}$ is the WIMP velocity in the galactic frame and $\mathbf{v}_E$ is the Earth velocity in the galactic frame, we use a Maxwell-Boltzmann velocity distribution as parameterized in the standard halo model, i.e., $v_0 = 220$ km/s, $v_E = 232$ km/s, $v_{esc} = 544$ km/s. The WIMP-nucleus cross section reads as

$$\sigma(E_R) = \frac{4}{3}\frac{\pi}{2J_i+1}\left(\frac{\mu}{\mu_{nucleon}}\right)\sigma_{nucleon}S_A(E_R), \quad (13)$$

with μ and $\mu_{nucleon}$ the reduced masses of the WIMP-nucleus and WIMP-nucleon systems, respectively. For the unknown spin-dependent WIMP-nucleon cross section we employ a value of $\sigma_{nucleon} = 10^{-40}$ cm^2. The resulting recoil spectra using "neutron-only" couplings, $S_A(E_R) = S_n(E_R)$, are shown in Fig. 3 for WIMP masses of 100 GeV and 200 GeV.

In Fig. 3 we see that inelastic scattering competes with elastic scattering at recoil energies $E_R \gtrsim 10$ keV. We note that the scale of the differential event rate is set by the unknown spin-dependent WIMP-nucleon cross section, and therefore the shape and relative magnitude of the elastic and inelastic event rates are interesting here instead of absolute numbers. It is also noteworthy that the lowest nuclear recoil energies would in reality be cut off by the detector threshold energy. Therefore, inelastic scattering could be an interesting signal for a detector sensitive to spin-dependent scattering solely through ^{183}W if the WIMPs are sufficiently heavy. The question whether building such a detector would be feasible or not, we leave for others to decide.

As a final remark, the shell-model prediction of Ref. [11] for ^{129}Xe gives a differential inelastic scattering event rate larger than that obtained for ^{183}W in the present work over a large range of roughly 15 keV $< E_R <$ 150 keV. The peak for ^{183}W is quite narrow at $E_R \approx 10$ keV whereas ^{129}Xe has a broader peak around

Table A.1
Fits to the spin structure functions for elastic WIMP-nucleus scattering off ^{183}W. The functions are fit in the form $S_{p/n}(u) = e^{-u}\sum_{i=0}^{13}\tilde{c}_i u^i$, where $u = q^2b^2/2 = m_A b^2 E_R$ is the recoil energy E_R in a dimensionless form with $b = 2.4069$ fm and m_A the mass of the nucleus. The fits are valid and accurate to within 1% up to $u = 8.0$ ($E_R = 310$ keV). Fits are given for lower and upper limits of the proton-only and neutron-only structure functions S_p and S_n both for $c_D = 0$ and the range $c_D = -8.0...2.0$.

	Fit parameters $\tilde{c}_i$ for $c_D = 0$			
i	S_p min	S_p max	S_n min	S_n max
0	4.0628026E-05	1.7043047E-04	6.9641478E-03	8.1206558E-03
1	3.2268168E-05	−5.9760629E-04	−2.3236565E-02	−2.8991097E-02
2	5.4206163E-04	2.9883154E-03	5.5688850E-02	7.3363724E-02
3	−2.5496629E-05	−3.5671618E-03	−6.6981154E-02	−9.3658929E-02
4	−8.4409679E-04	1.6828590E-03	4.4066291E-02	6.6632663E-02
5	7.8429897E-04	−1.2540494E-04	−1.7450277E-02	−2.9043286E-02
6	−3.1543751E-04	−2.3265687E-04	4.5249081E-03	8.2291122E-03
7	5.9975831E-05	1.2755383E-04	−8.5989044E-04	−1.5639590E-03
8	−1.9927959E-06	−3.5297595E-05	1.3915477E-04	1.9979421E-04
9	−1.4461700E-06	6.1760977E-06	−2.0308508E-05	−1.6290587E-05
10	3.1606502E-07	−7.1272539E-07	2.3685540E-06	6.8150836E-07
11	−3.0801613E-08	5.2708400E-08	−1.8697783E-07	4.6628214E-09
12	1.5174806E-09	−2.2588652E-09	8.5216601E-09	−1.7823171E-09
13	−3.0682710E-11	4.2508593E-11	−1.6763274E-10	5.4729104E-11
	Fit parameters $\tilde{c}_i$ for $c_D = -8.0...2.0$			
i	S_p min	S_p max	S_n min	S_n max
0	3.9311863E-05	1.7115940E-04	6.9595903E-03	8.1401654E-03
1	−9.0549775E-06	−5.8434165E-04	−2.3338677E-02	−2.8572328E-02
2	4.8290690E-04	3.0629340E-03	5.5532621E-02	7.3129846E-02
3	−2.5581378E-04	−3.6160702E-03	−6.6583326E-02	−9.2018840E-02
4	−2.8136857E-04	1.6120871E-03	4.3759207E-02	6.2872488E-02
5	2.9930161E-04	−1.5767775E-05	−1.7332136E-02	−2.5234673E-02
6	−9.0795222E-05	−3.0008894E-04	4.5017959E-03	6.0262095E-03
7	−2.5072909E-06	1.5175386E-04	−8.5866339E-04	−7.5683664E-04
8	8.6938420E-06	−4.0897077E-05	1.3957384E-04	3.8411073E-06
9	−2.5287693E-06	7.0425176E-06	−2.0412545E-05	1.5694760E-05
10	3.7027537E-07	−8.0245682E-07	2.3796742E-06	−2.7921324E-06
11	−3.0761458E-08	5.8705919E-08	−1.8762349E-07	2.4535925E-07
12	1.3863254E-09	−2.4932804E-09	8.5412640E-09	−1.1409277E-08
13	−2.6457518E-11	4.6581547E-11	−1.6787279E-10	2.2378186E-10

$E_R \approx 30$ keV. Therefore advantages of using ^{183}W over xenon in a detector are not obvious and would have to originate from the shape of the recoil spectrum or the elastic/inelastic scattering ratio.

5. Summary and conclusions

We have reported the first calculation of spin-dependent structure functions for WIMP-nucleus scattering for the deformed ^{183}W nucleus. Our results include the leading effects of two-body currents derived from chiral EFT, and the nuclear-structure calculations were performed in a reliable microscopic nuclear framework of IBFM-2.

We confirm the earlier expectation of suppressed detection possibilities via spin-dependent elastic scattering. For inelastic scattering, however, we find the important "neutron-only" structure function to be sizable especially for small momentum transfers. Moreover, the inelastic-scattering structure function dominates over the elastic-scattering structure function for all momentum transfers. This makes ^{183}W to our knowledge the first nucleus studied where inelastic scattering could be the dominant experimental signal. However, judging by the estimated recoil spectra, there seem to be no obvious advantages of using ^{183}W instead of xenon, for example.

Our results are of interest to the CRESST collaboration and possible future detectors using tungsten in one form or other. A study to estimate the spin-independent scattering response of all stable W isotopes will follow. The framework of the present work will also be applied to other heavy deformed nuclei that could be used in future detectors.

Declaration of competing interest

The authors declare the following financial interests/personal relationships which may be considered as potential competing interests:

This work was supported by the Academy of Finland under Project No. 318043. The work of JK was supported by the Academy of Finland (Grant Nos. 314733 and 320062).

Acknowledgements

This work was supported by the Academy of Finland under Project No. 318043. The work of JK was supported by the Academy of Finland (Grant Nos. 314733 and 320062).

Appendix A. Fits to spin structure functions

In this appendix we provide fits to the spin structure functions shown in Fig. 2. The fit parameters for S_p and S_n for elastic and inelastic scattering are given in Tables A.1 and A.2, respectively.

References

[1] E. Aprile, J. Aalbers, F. Agostini, M. Alfonsi, L. Althueser, F.D. Amaro, M. Anthony, F. Arneodo, L. Baudis, B. Bauermeister, M.L. Benabderrahmane, T. Berger, P.A. Breur, A. Brown, A. Brown, E. Brown, S. Bruenner, G. Bruno, R. Budnik, C. Capelli, J.M.R. Cardoso, D. Cichon, D. Coderre, A.P. Colijn, J. Conrad, J.P. Cussonneau, M.P. Decowski, P. de Perio, P. Di Gangi, A. Di Giovanni, S. Diglio, A. Elykov, G. Eurin, J. Fei, A.D. Ferella, A. Fieguth, W. Fulgione, A. Gallo Rosso, M. Galloway, F. Gao, M. Garbini, C. Geis, L. Grandi, Z. Greene, H. Qiu, C. Hasterok, E. Hogenbirk, J. Howlett, R. Itay, F. Joerg, B. Kaminsky, S. Kazama, A. Kish, G. Koltman, H. Landsman, R.F. Lang, L. Levinson, Q. Lin, S. Lindemann, M. Lindner, F. Lombardi, J.A.M. Lopes, J. Mahlstedt, A. Manfredini, T. Marrodán Undagoitia, J. Masbou, D. Masson, M. Messina, K. Micheneau, K. Miller, A. Molinario, K. Morå,

Table A.2
Same as Table A.1 but for inelastic scattering.

	Fit parameters $\tilde{c}_i$ for $c_D = 0$			
i	S_p min	S_p max	S_n min	S_n max
0	1.1541016E-04	4.6107254E-04	1.8330374E-02	2.1347646E-02
1	−7.4033802E-05	−1.3057754E-03	−6.2671503E-02	−7.4896303E-02
2	1.9196116E-03	5.3175913E-03	1.2610497E-01	1.5636725E-01
3	−2.5643292E-03	−7.1539000E-03	−1.3866333E-01	−1.8379809E-01
4	1.1138779E-03	4.7599179E-03	8.8094267E-02	1.3152582E-01
5	−2.1130042E-04	−2.1897267E-03	−3.3815932E-02	−6.2132540E-02
6	1.2440556E-04	9.0531722E-04	7.8796100E-03	2.0740850E-02
7	−9.7358848E-05	−3.2171216E-04	−1.0083310E-03	−5.1246516E-03
8	3.8086483E-05	8.4068645E-05	2.5219665E-05	9.5350491E-04
9	−8.3481302E-06	−1.4888691E-05	1.4258744E-05	−1.3160143E-04
10	1.0990465E-06	1.7207270E-06	−2.6421510E-06	1.2920317E-05
11	−8.6871347E-08	−1.2404284E-07	2.2850136E-07	−8.4304113E-07
12	3.8153744E-09	5.0621079E-09	−1.0358116E-08	3.2491605E-08
13	−7.1761082E-11	−8.9334987E-11	1.9801732E-10	−5.5667132E-10
	Fit parameters $\tilde{c}_i$ for $c_D = -8.0...2.0$			
i	S_p min	S_p max	S_n min	S_n max
0	1.1171785E-04	4.6296577E-04	1.8318307E-02	2.1399771E-02
1	−1.6148035E-04	−1.2616204E-03	−6.2921343E-02	−7.4037790E-02
2	2.2289516E-03	5.1051399E-03	1.2756169E-01	1.5120805E-01
3	−2.9256834E-03	−6.7419319E-03	−1.4192336E-01	−1.7212785E-01
4	1.1941350E-03	4.3182923E-03	9.2023658E-02	1.1735971E-01
5	−1.1204481E-05	−1.8983577E-03	−3.6706721E-02	−5.1648625E-02
6	−9.8198636E-05	7.8053263E-04	9.2658241E-03	1.5685423E-02
7	1.5427874E-05	−2.8584467E-04	−1.4583603E-03	−3.4745391E-03
8	4.3647429E-06	7.7020025E-05	1.2598405E-04	5.8210777E-04
9	−1.9769259E-06	−1.3939425E-05	−1.3183729E-06	−7.3904997E-05
10	3.2883753E-07	1.6347129E-06	−1.0104029E-06	6.8490646E-06
11	−2.9005877E-08	−1.1905059E-07	1.1804384E-07	−4.3037800E-07
12	1.3514010E-09	4.8955553E-09	−6.0043001E-09	1.6166542E-08
13	−2.6286672E-11	−8.6928771E-11	1.2222857E-10	−2.7157319E-10

M. Murra, J. Naganoma, K. Ni, U. Oberlack, B. Pelssers, F. Piastra, J. Pienaar, V. Pizzella, G. Plante, R. Podviianiuk, N. Priel, D. Ramírez García, L. Rauch, S. Reichard, C. Reuter, B. Riedel, A. Rizzo, A. Rocchetti, N. Rupp, J.M.F. dos Santos, G. Sartorelli, M. Scheibelhut, S. Schindler, J. Schreiner, D. Schulte, M. Schumann, L. Scotto Lavina, M. Selvi, P. Shagin, E. Shockley, M. Silva, H. Simgen, D. Thers, F. Toschi, G. Trinchero, C. Tunnell, N. Upole, M. Vargas, O. Wack, H. Wang, Z. Wang, Y. Wei, C. Weinheimer, C. Wittweg, J. Wulf, J. Ye, Y. Zhang, T. Zhu, Dark matter search results from a one ton-year exposure of XENON1T, Phys. Rev. Lett. 121 (2018) 111302, https://doi.org/10.1103/PhysRevLett.121.111302, https://link.aps.org/doi/10.1103/PhysRevLett.121.111302.

[2] D.S. Akerib, C.W. Akerlof, S.K. Alsum, H.M. Araújo, M. Arthurs, X. Bai, A.J. Bailey, J. Balajthy, S. Balashov, D. Bauer, J. Belle, P. Beltrame, T. Benson, E.P. Bernard, T.P. Biesiadzinski, K.E. Boast, B. Boxer, P. Brás, J.H. Buckley, V.V. Bugaev, S. Burdin, J.K. Busenitz, C. Carels, D.L. Carlsmith, B. Carlson, M.C. Carmona-Benitez, C. Chan, J.J. Cherwinka, A. Cole, A. Cottle, W.W. Craddock, A. Currie, J.E. Cutter, C.E. Dahl, L. de Viveiros, A. Dobi, J.E.Y. Dobson, E. Druszkiewicz, T.K. Edberg, W.R. Edwards, A. Fan, S. Fayer, S. Fiorucci, T. Fruth, R.J. Gaitskell, J. Genovesi, C. Ghag, M.G.D. Gilchriese, M.G.D. van der Grinten, C.R. Hall, S. Hans, K. Hanzel, S.J. Haselschwardt, S.A. Hertel, S. Hillbrand, C. Hjemfelt, M.D. Hoff, J.Y.-K. Hor, D.Q. Huang, C.M. Ignarra, W. Ji, A.C. Kaboth, K. Kamdin, J. Keefner, D. Khaitan, A. Khazov, Y.D. Kim, C.D. Kocher, E.V. Korolkova, H. Kraus, H.J. Krebs, L. Kreczko, B. Krikler, V.A. Kudryavtsev, S. Kyre, J. Lee, B.G. Lenardo, D.S. Leonard, K.T. Lesko, C. Levy, J. Li, J. Liao, F.-T. Liao, J. Lin, A. Lindote, R. Linehan, W.H. Lippincott, X. Liu, M.I. Lopes, B. López Paredes, W. Lorenzon, S. Luitz, J.M. Lyle, P. Majewski, A. Manalaysay, R.L. Mannino, C. Maupin, D.N. McKinsey, Y. Meng, E.H. Miller, J. Mock, M.E. Monzani, J.A. Morad, E. Morrison, B.J. Mount, A.S.J. Murphy, H.N. Nelson, F. Neves, J. Nikoleyczik, K. O'Sullivan, I. Olcina, M.A. Olevitch, K.C. Oliver-Mallory, K.J. Palladino, S.J. Patton, E.K. Pease, B. Penning, A. Piepke, S. Powell, R.M. Preece, K. Pushkin, B.N. Ratcliff, J. Reichenbacher, C.A. Rhyne, A. Richards, J.P. Rodrigues, R. Rosero, P. Rossiter, J.S. Saba, M. Sarychev, R.W. Schnee, M. Schubnell, P.R. Scovell, S. Shaw, T.A. Shutt, J.J. Silk, C. Silva, K. Skarpaas, W. Skulski, M. Solmaz, V.N. Solovov, P. Sorensen, I. Stancu, M.R. Stark, T.M. Stiegler, K. Stifter, M. Szydagis, W.C. Taylor, R. Taylor, D.J. Taylor, D. Temples, P.A. Terman, K.J. Thomas, M. Timalsina, W.H. To, A. Tomás, T.E. Tope, M. Tripathi, C.E. Tull, L. Tvrznikova, U. Utku, J. Va'vra, A. Vacheret, J.R. Verbus, E. Voirin, W.L. Waldron, J.R. Watson, R.C. Webb, D.T. White, T.J. Whitis, W.J. Wisniewski, M.S. Witherell, F.L.H. Wolfs, D. Woodward, S.D. Worm, M. Yeh, J. Yin, I. Young, Projected WIMP sensitivity of the LUX-ZEPLIN dark matter experiment, Phys. Rev. D 101 (2020) 052002, https://doi.org/10.1103/PhysRevD.101.052002, https://link.aps.org/doi/10.1103/PhysRevD.101.052002.

[3] M.T. Ressell, M.B. Aufderheide, S.D. Bloom, K. Griest, G.J. Mathews, D.A. Resler, Nuclear shell model calculations of neutralino-nucleus cross sections for ^{29}Si and ^{73}Ge, Phys. Rev. D 48 (1993) 5519–5535, https://doi.org/10.1103/PhysRevD.48.5519, https://link.aps.org/doi/10.1103/PhysRevD.48.5519.

[4] M.T. Ressell, D.J. Dean, Spin-dependent neutralino-nucleus scattering for $A \sim 127$ nuclei, Phys. Rev. C 56 (1997) 535–546, https://doi.org/10.1103/PhysRevC.56.535, https://link.aps.org/doi/10.1103/PhysRevC.56.535.

[5] P.C. Divari, T.S. Kosmas, J.D. Vergados, L.D. Skouras, Shell model calculations for light supersymmetric particle scattering off light nuclei, Phys. Rev. C 61 (2000) 054612, https://doi.org/10.1103/PhysRevC.61.054612, https://link.aps.org/doi/10.1103/PhysRevC.61.054612.

[6] E. Holmlund, M. Kortelainen, T. Kosmas, J. Suhonen, J. Toivanen, Microscopic calculation of the LSP detection rates for the 71Ga, 73Ge and 127I dark-matter detectors, Phys. Lett. B 584 (1) (2004) 31–39, https://doi.org/10.1016/j.physletb.2004.01.045, http://www.sciencedirect.com/science/article/pii/S0370269304001789.

[7] M. Kortelainen, T. Kosmas, J. Suhonen, J. Toivanen, Event rates for CDM detectors from large-scale shell-model calculations, Phys. Lett. B 632 (2) (2006) 226–232, https://doi.org/10.1016/j.physletb.2005.10.057, http://www.sciencedirect.com/science/article/pii/S0370269305015467.

[8] P. Toivanen, M. Kortelainen, J. Suhonen, J. Toivanen, Large-scale shell-model calculations of elastic and inelastic scattering rates of lightest supersymmetric particles (LSP) on ^{127}I, ^{129}Xe, ^{131}Xe, and ^{133}Cs nuclei, Phys. Rev. C 79 (2009) 044302, https://doi.org/10.1103/PhysRevC.79.044302, https://link.aps.org/doi/10.1103/PhysRevC.79.044302.

[9] J. Menéndez, D. Gazit, A. Schwenk, Spin-dependent WIMP scattering off nuclei, Phys. Rev. D 86 (2012) 103511, https://doi.org/10.1103/PhysRevD.86.103511, https://link.aps.org/doi/10.1103/PhysRevD.86.103511.

[10] P. Klos, J. Menéndez, D. Gazit, A. Schwenk, Large-scale nuclear structure calculations for spin-dependent WIMP scattering with chiral effective field theory currents, Phys. Rev. D 88 (2013) 083516, https://doi.org/10.1103/PhysRevD.88.083516, https://link.aps.org/doi/10.1103/PhysRevD.88.083516.

[11] L. Baudis, G. Kessler, P. Klos, R.F. Lang, J. Menéndez, S. Reichard, A. Schwenk, Signatures of dark matter scattering inelastically off nuclei, Phys. Rev. D 88 (2013) 115014, https://doi.org/10.1103/PhysRevD.88.115014, https://link.aps.org/doi/10.1103/PhysRevD.88.115014.

[12] L. Vietze, P. Klos, J. Menéndez, W.C. Haxton, A. Schwenk, Nuclear structure aspects of spin-independent WIMP scattering off xenon, Phys. Rev. D 91 (2015) 043520, https://doi.org/10.1103/PhysRevD.91.043520, https://link.aps.org/doi/10.1103/PhysRevD.91.043520.

[13] P. Pirinen, P.C. Srivastava, J. Suhonen, M. Kortelainen, Shell-model study on event rates of lightest supersymmetric particles scattering off ^{83}Kr and ^{125}Te,

Phys. Rev. D 93 (2016) 095012, https://doi.org/10.1103/PhysRevD.93.095012, https://link.aps.org/doi/10.1103/PhysRevD.93.095012.
[14] A.L. Fitzpatrick, W. Haxton, E. Katz, N. Lubbers, Y. Xu, The effective field theory of dark matter direct detection, J. Cosmol. Astropart. Phys. 2013 (02) (2013) 004, https://doi.org/10.1088/1475-7516/2013/02/004, https://doi.org/10.1088/1475-7516/2013/02/004.
[15] F. Giuliani, T.A. Girard, Model-independent limits from spin-dependent WIMP dark matter experiments, Phys. Rev. D 71 (2005) 123503, https://doi.org/10.1103/PhysRevD.71.123503, https://link.aps.org/doi/10.1103/PhysRevD.71.123503.
[16] P. Pirinen, J. Kotila, J. Suhonen, Spin-dependent wimp-nucleus scattering off 125Te, 129Xe, and 131Xe in the microscopic interacting boson-fermion model, Nucl. Phys. A 992 (2019) 121624, https://doi.org/10.1016/j.nuclphysa.2019.121624, http://www.sciencedirect.com/science/article/pii/S037594741930199X.
[17] M. Hoferichter, P. Klos, A. Schwenk, Chiral power counting of one- and two-body currents in direct detection of dark matter, Phys. Lett. B 746 (2015) 410–416, https://doi.org/10.1016/j.physletb.2015.05.041, http://www.sciencedirect.com/science/article/pii/S0370269315003780.
[18] M. Hoferichter, J. Menéndez, A. Schwenk, Coherent elastic neutrino-nucleus scattering: EFT analysis and nuclear responses, Phys. Rev. D 102 (2020) 074018, https://doi.org/10.1103/PhysRevD.102.074018, https://link.aps.org/doi/10.1103/PhysRevD.102.074018.
[19] J. Engel, S. Pittel, P. Vogel, Nuclear physics of dark matter detection, Int. J. Mod. Phys. E 01 (01) (1992) 1–37, https://doi.org/10.1142/S0218301392000023, https://doi.org/10.1142/S0218301392000023.
[20] B. Märkisch, H. Mest, H. Saul, X. Wang, H. Abele, D. Dubbers, M. Klopf, A. Petoukhov, C. Roick, T. Soldner, D. Werder, Measurement of the weak axial-vector coupling constant in the decay of free neutrons using a pulsed cold neutron beam, Phys. Rev. Lett. 122 (2019) 242501, https://doi.org/10.1103/PhysRevLett.122.242501, https://link.aps.org/doi/10.1103/PhysRevLett.122.242501.
[21] V. Bernard, N. Kaiser, U.-G. Meissner, Aspects of chiral pion-nucleon physics, Nucl. Phys. A 615 (4) (1997) 483–500, https://doi.org/10.1016/S0375-9474(97)00021-3, http://www.sciencedirect.com/science/article/pii/S0375947497000213.
[22] M. Hoferichter, J. Ruiz de Elvira, B. Kubis, U.-G. Meißner, Matching pion-nucleon Roy-Steiner equations to chiral perturbation theory, Phys. Rev. Lett. 115 (2015) 192301, https://doi.org/10.1103/PhysRevLett.115.192301, https://link.aps.org/doi/10.1103/PhysRevLett.115.192301.
[23] J. Menéndez, D. Gazit, A. Schwenk, Chiral two-body currents in nuclei: Gamow-Teller transitions and neutrinoless double-beta decay, Phys. Rev. Lett. 107 (2011) 062501, https://doi.org/10.1103/PhysRevLett.107.062501, https://link.aps.org/doi/10.1103/PhysRevLett.107.062501.
[24] L.-J. Wang, J. Engel, J.M. Yao, Quenching of nuclear matrix elements for $0\nu\beta\beta$ decay by chiral two-body currents, Phys. Rev. C 98 (2018) 031301, https://doi.org/10.1103/PhysRevC.98.031301, https://link.aps.org/doi/10.1103/PhysRevC.98.031301.
[25] A. Baroni, R. Schiavilla, L.E. Marcucci, L. Girlanda, A. Kievsky, A. Lovato, S. Pastore, M. Piarulli, S.C. Pieper, M. Viviani, R.B. Wiringa, Local chiral interactions, the tritium Gamow-Teller matrix element, and the three-nucleon contact term, Phys. Rev. C 98 (2018) 044003, https://doi.org/10.1103/PhysRevC.98.044003, https://link.aps.org/doi/10.1103/PhysRevC.98.044003.
[26] F. Sammarruca, L.E. Marcucci, L. Coraggio, J.W. Holt, N. Itaco, R. Machleidt, Nuclear and neutron matter equations of state from high-quality potentials up to fifth order of the chiral expansion, arXiv:1807.06640, 2018.
[27] P. Navratil, B.R. Barrett, J. Dobeš, M1 properties of tungsten isotopes in the interacting boson model-2, Phys. Rev. C 53 (6) (1996) 2794.
[28] J. Kotila, J. Barea, Occupation probabilities of single particle levels using the microscopic interacting boson model: application to some nuclei of interest in neutrinoless double-β decay, Phys. Rev. C 94 (2016) 034320, https://doi.org/10.1103/PhysRevC.94.034320, https://link.aps.org/doi/10.1103/PhysRevC.94.034320.
[29] S. Abu Musleh, O. Scholten, A description of odd mass W-isotopes in the interacting boson-fermion model, Nucl. Phys. A 878 (2012) 37–48, https://doi.org/10.1016/j.nuclphysa.2012.01.011, http://www.sciencedirect.com/science/article/pii/S0375947412000425.
[30] J. Barea, C. Alonso, J. Arias, The one nucleon transfer operator in the microscopic IBM without NOA, Phys. Lett. B 737 (2014) 205–209, https://doi.org/10.1016/j.physletb.2014.08.026, http://www.sciencedirect.com/science/article/pii/S0370269314005930.
[31] A. Arima, T. Ohtsuka, F. Iachello, I. Talmi, Collective nuclear states as symmetric couplings of proton and neutron excitations, Phys. Lett. B 66 (3) (1977) 205–208, https://doi.org/10.1016/0370-2693(77)90860-7, http://www.sciencedirect.com/science/article/pii/0370269377908607.
[32] T. Otsuka, A. Arima, F. Iachello, Nuclear shell model and interacting bosons, Nucl. Phys. A 309 (1) (1978) 1–33, https://doi.org/10.1016/0375-9474(78)90532-8, http://www.sciencedirect.com/science/article/pii/0375947478905328.
[33] J. Barea, F. Iachello, Neutrinoless double-β decay in the microscopic interacting boson model, Phys. Rev. C 79 (2009) 044301, https://doi.org/10.1103/PhysRevC.79.044301, https://link.aps.org/doi/10.1103/PhysRevC.79.044301.
[34] C.M. Baglin, Nuclear data sheets for A = 183, Nucl. Data Sheets 134 (2016) 149–430, https://doi.org/10.1016/j.nds.2016.04.002, http://www.sciencedirect.com/science/article/pii/S0090375216300023.
[35] P. Smith, J. Lewin, Dark matter detection, Phys. Rep. 187 (5) (1990) 203–280, https://doi.org/10.1016/0370-1573(90)90081-C, https://www.sciencedirect.com/science/article/pii/037015739090081C.